Magnetic Resonance in Medicine 54:1387–1396 (2005)

Dependence on Diffusion Time of Apparent Diffusion Tensor of Ex Vivo Calf Tongue and Heart

Sungheon Kim,[1]* Gloria Chi-Fishman,[1] Alan S. Barnett,[2] and Carlo Pierpaoli[3]

The time dependence of the apparent diffusion tensor of ex vivo calf heart and tongue was measured for diffusion times (τ_d) between 32 and 810 ms. The results showed evidence of restricted diffusion in the muscle tissues of both organs. In regions where the myofibers are parallel, the largest eigenvalue (λ_1) of the diffusion tensor remained the same for all diffusion times measured, while the other eigenvalues (λ_2, λ_3) decreased by 29–36% between τ_d = 32 ms and τ_d = 400 ms. In regions where the fibers cross, the λ_1 also changed, decreasing by 17% between τ_d = 32 ms and τ_d = 400 ms. The restricting compartment size and volume fraction were effectively estimated by fitting the time courses of the eigenvalues to a model consisting of a nonrestricted compartment and a cylindrically restricted compartment. To our knowledge, this study is the first demonstrating diffusion time dependence of measured water diffusion tensor in muscular tissue. With improvement in scanning technology, future studies may permit noninvasive, in vivo detection of changes in muscle myoarchitecture due to disease, treatment, and exercise. Magn Reson Med 54:1387–1396, 2005. Published 2005 Wiley-Liss, Inc.†

Key words: DTI; restricted water diffusion; tongue; heart; diffusion time

The anisotropy and reduction of intracellular water diffusion in skeletal muscle compared to free water diffusion based on diffusion-weighted nuclear magnetic resonance measurements was first reported by Cleveland et al. (1) in 1976. Since then, diffusion-weighted nuclear magnetic resonance spectroscopy (DW-MRS) has been used to study diffusion anisotropy induced by subcellular or cellular structures in muscles (2,3). The more powerful technique of diffusion tensor imaging (DTI) (4) also has been used to study the myoarchitecture of skeletal muscle (4–7) as well as more complex muscular organs such as the heart (9–12) and the tongue (13–15).

van Donkelaar et al. (5) used DTI to generate a finite element mesh model to study skeletal muscle function. Sinha and Yao (6) used DTI with a tetrahedral encoding scheme to measure the anisotropy of water diffusion in in vivo human calf muscle and to map the elevation and azimuth angles of muscle fibers. Damon et al. (7) used DTI to measure the pennation angle in the skeletal muscle of rat and found the DTI-derived values to be highly correlated (r = 0.89) with measurement by direct anatomic inspection. In the future, it may become possible to use DTI to monitor the progression of musculoskeletal diseases or the effect of exercise.

Quantitative validation of DTI-based fiber orientation measurement has also been performed for the myocardium (8). Although cardiac muscle fiber is less striated than skeletal muscle fiber, DTI and histologic measurement of fiber orientation by Holmes et al. (8) differed on average by only 3.7°. Scollan et al. (9) demonstrated the utility of DTI for the study of myoarchitecture by visualizing the complex laminar structure of cardiac ventricles using maps of inclination angle and eigenvectors. Winslow et al. (10) used the estimated diffusion tensors to reconstruct the geometry of the ventricles with potential application in studying the electrical excitation of the heart. Dou et al. (11) used bipolar diffusion gradients for in vivo human cardiac DTI with reduced strain effect, while Chen et al. (12) used DTI to study structural changes due to myocardial infarction.

Although DTI has been used to visualize the complex myoarchitecture of the tongue (13–15), only qualitative validation has been attempted to show the accuracy of DTI for the estimation of fiber orientation. A unique feature of lingual myoarchitecture is the heavily interwoven laminar structure of the muscle fibers in the intrinsic core region. Wedeen et al. (14) found the diffusion tensor in this region to be oblate with the eigenvector corresponding to the smallest eigenvalue oriented perpendicular to the plane containing the fibers. However, the capability of DTI to map the complex lingual myoarchitecture in detail and its usefulness for studying the effect of lingual pathology on swallowing and speech have not been demonstrated to date.

In previous DTI studies of muscular organs, the diffusion time (time delay between the two diffusion sensitizing gradient pulses, τ_d) was kept constant, and the possible dependence of water diffusivity on diffusion time was not investigated. In the experiments described above, τ_d for heart and skeletal muscle measurements was 20 to 35 ms, while τ_d for tongue muscle measurements was 45 to 500 ms.

Dependence of diffusivity on τ_d indicates the presence of barriers that restrict the otherwise free diffusion. In the original formulation of Woessner (16) the barriers are modeled as impenetrable (representing macromolecules or small dense organelles), whereas in the formulation of Crick (17) the barriers are permeable (representing, for instance, the cell membrane). More recent studies have investigated in detail the relationship between diffusion

[1]Physical Disabilities Branch, Department of Rehabilitation Medicine, Clinical Research Center, National Institutes of Health, Bethesda, Maryland, USA.

[2]National Institute of Mental Health, National Institutes of Health, Bethesda, Maryland, USA.

[3]National Institute of Child Health and Human Development, National Institutes of Health, Bethesda, Maryland, USA.

The opinions presented in this report reflect the views of the authors and not those of the National Institutes of Health nor the US Public Health Service.

*Correspondence to: Sungheon Kim, Physical Disabilities Branch, Department of Rehabilitation Medicine, Clinical Research Center, National Institutes of Health, 10/6c416, 10 Center Drive, Bethesda, MD 20892-1391, USA. E-mail: sungheonk@cc.nih.gov

Received 11 February 2005; revised 4 May 2005; accepted 8 July 2005.

DOI 10.1002/mrm.20676

Published online 1 November 2005 in Wiley InterScience (www.interscience.wiley.com).

time dependence and the size of the restricting compartment (18–21). If τ_d is sufficiently short, a very small fraction of the diffusing particles encounters a barrier, so the measured diffusivity is that of the bulk fluid. As τ_d approaches the time required for a particle to diffuse a distance comparable to the spacing between the barriers, the number of particles that encounter the barriers increases, and the average displacement of the particles, hence the diffusivity, decreases. The characteristic time τ_r for restrictive effects is therefore $\sim L^2/D$, where L is a distance typical of the spacing between the barriers and D is the diffusivity of the bulk fluid. For neurons in the brain, the diameter of the axons is $\sim$1 μm, $D \sim 1$ μm^2/ms, and $\tau_r \sim 1$ ms. Since the shortest diffusion time achievable for in vivo studies is $\sim$20 ms, it is therefore not surprising that diffusion time dependence is not observed in these studies when $\tau_d >$ 6 ms. As the diameter of muscle cells is $\sim$10 μm, and $\tau_r \sim$ 100 ms, observation of the effects of restriction is expected at an achievable τ_d. Such effects have in fact been observed in ^{31}P DW-MRS studies of phosphorous-containing compounds in muscle tissues (2,3).

The purpose of the present work is to observe restricted diffusion of water in muscle tissue by varying τ_d between 32 and 800 ms. This range was chosen to study the effects of restriction, given an expected τ_r on the order of 100 ms. The heart and the tongue were chosen as target specimens because of the unique arrangement of muscle fibers in these organs. DTI was used instead of DW-MRS for improved localization and correlation with anatomy. A simple two-component diffusion model was developed to estimate the size of the restrictive compartments.

METHODS

Specimens

Our specimens included four excised calf hearts and four excised calf tongues acquired en bloc from a USDA-approved commercial slaughterhouse (Baltimore, MD, USA) within 2 h of slaughter. The specimens were wrapped in polyethylene wrap to avoid dehydration and refrigerated. To minimize temperature changes during the scans, we brought the specimens to room temperature at least 4 h before scanning. The specimens were scanned in less than 24 h after harvest.

MR Data Acquisition and Postprocessing

All scanning took place in a 1.5 T GE Signa MR scanner (GE Medical Systems, Milwaukee, WI, USA) equipped with a whole-body gradient coil producing gradient pulses up to 50 mT/m, using a standard clinical quadrature head coil. A custom diffusion-sensitive stimulated-echo (STEAM) pulse sequence was used with eight-shot echo-planar spatial encoding. The STEAM sequence reduces the signal loss due to T_2 decay, while the eight-shot EPI readout is a good compromise between the T_2 losses and spatial distortion of single-shot EPI and the excessive scan time of a conventional acquisition. Our acquisition matrix was 128 × 64 for an FOV of 260 × 130 mm with 2-mm slice thickness, yielding a spatial resolution of 2.03 × 2.03 × 2 mm^3. To improve S/N, each acquisition was repeated eight times. For the tongue specimens, we selected slices with 20-mm spacing perpendicular to the direction from the tip to the base of the tongue. For the heart specimens, we selected four short axis slices with 20-mm spacing. The repetition time (TR) was 3.0 s. In addition to a reference image with no diffusion pulses, images were acquired with diffusion pulses in six different directions; [1,1,0], [1,0,1], [0,1,1], [1, −1, 0], [1, 0, −1], and [0, 1, −1]. To reduce the effect of imaging gradients, images were also acquired with the polarity of the diffusion gradients reversed. Each data set therefore consisted of 104 images, eight repetitions each of 13 gradient directions.

To investigate the effect of diffusion time on the computed water diffusivity, an experimental design was implemented that held the diffusion weighting (the b matrix) constant. The diffusion time was changed by changing the mixing time (TM) (the time between the second and third RF pulses) from 10 to 800 ms, resulting in diffusion times ranging from 32 to 810 ms. The trace of the b-matrix was kept constant at about 1400 s/mm^2 by varying the width of the diffusion weighting gradients from 14.4 to 2.4 ms (TE = 47.9 to 23.9 ms). The amplitude of the diffusion gradient was 44.5 mT/m for all diffusion-weighted scans. The total scan time was about 10 h 30 min.

The acquired images were reconstructed using software written in IDL (Research Systems, Inc.). The diffusion tensor was computed for each voxel using a nonlinear fitting method with noise estimation to minimize the effect of outliers (22). Subsequently, the eigenvalues and eigenvectors of each tensor were calculated. The results were used to compute fractional anisotropy (FA) (23), skewness (SK) (24), and lattice index (LI) (25), with averaging of the diffusion parameters over regions of interest (ROI) chosen to have homogeneous muscle fiber structure. Visualization of the muscles or muscle groups and their orientations was accomplished through directionally encoded color (DEC) maps (26).

Experiments to Control for Potential Confounds

Effects of imaging gradients

Our computation of the b-matrix factored in the contribution of imaging gradients to the diffusion sensitization. After discovering the important contribution of the slice select gradients and the crushers for long τ_d scans, we modified the amplitude of the z-diffusion gradient whenever possible to compensate for the slice select gradient. Since the crushers were used for the z-diffusion gradient, the contribution of the crushers was only important for acquisitions for which no z-diffusion weighting was desired. To optimize the sequence in this case, a series of experiments was carried out to assess the minimum strength of the crusher gradients needed to obtain artifact-free images. Some acquired images had the polarity of the slice select gradients reversed with respect to the diffusion gradients. The error introduced in the diffusion time by the slice select contribution was negligible because (i) for short τ_d the contribution of the slice select gradients was small, and (ii) for large τ_d the time offset between the slice select gradient and the diffusion gradients was small compared to τ_d.

Accuracy of the STEAM Sequence

For all our clinical DTI studies we use a spin echo (SE) sequence whose results are periodically checked for accuracy in both phantoms and human subjects. To check for the possible presence of systematic errors in data produced with the less commonly used STEAM sequence, the diffusion tensor measured using the STEAM pulse sequence was compared with measurements obtained in the same object with the SE pulse sequence. Because of its sensitivity to T_2 relaxation, the SE pulse sequence cannot be used to study long diffusion times, whereas the STEAM pulse sequence cannot be used for short diffusion times due to the need for time to play out the three radiofrequency pulses and the associated gradients. Both sequences can be used for intermediate diffusion time. We compared the eigenvalues and anisotropy measures computed from a SE dataset with TE = 67.1 ms and τ_d = 36.6 ms with those computed from a STEAM dataset with TE = 57 ms and TM = 10 ms and the same diffusion time. The agreement was excellent; differences between the two methods were within 95% limits of agreement (27).

Effects of Echo Time (TE)

In order to maintain a constant *b*-value with increasing diffusion time, one must decrease either the width or the amplitude of the diffusion sensitizing gradients. We chose to decrease the width of the diffusion gradients and to keep their amplitude constant. While enabling shortening of TE and improvement of S/N at longer diffusion times, this strategy has the effect of producing different T_2 weighting for data acquired at different diffusion times. If the tissue has water pools with different T_2 values, the relative contributions of the pools to the signal will not be the same at all diffusion times due to the difference in the amount of T_2 decay, an undesirable effect. To check whether this effect was present in our tissue, parallel experiments were performed in one calf heart and one calf tongue by keeping constant either the gradient pulse width or the gradient pulse amplitude. For the constant amplitude experiment the gradient amplitude was kept at 44.5 mT/m, while for the constant width experiment the gradient pulse width was kept constant at 12.5 ms (TE = 43.7 ms).

Temperature Effects

Our specimens were kept at room temperature for more than 4 h prior to scanning, and the temperature of the scanner room was maintained at about 23°C. However, the temperature of the specimen could change due to RF heating during the long scan, thereby changing the sample diffusivity. To control for the possible temperature change, a scheme was adopted to acquire the data in blocks containing all the τ_d values. Testing of systematic changes in the measured tensor quantities was accomplished by comparing equivalent images taken at different times during the scan. In addition to temperature changes, such errors could be caused by the system.

Assumption of Monoexponential Decay

Our computation of the diffusion tensor from images acquired with only two levels of diffusion sensitization, b = 0 and b = 1400 s/mm^2, assumed a monoexponential decay of the signal as a function of b. To check whether the single tensor model was appropriate to fit the data within the range of *b*-values used for our experiment, a sample dataset was acquired in one calf heart and one calf tongue with multiple *b*-values at a single diffusion time of 400 ms. For this experiment, the *b*-values were 12, 110, 196, 599, 991, 1481, and 2070 s/mm^2, with 6, 10, 12, 16, 18, 20, and 22 gradient sampling orientations, respectively. For each *b*-value, the diffusion sampling orientations were selected according to the optimal strategy suggested by Jones et al. (28). The data were fitted to a number of different one or two tensor models, and the goodness of fit was evaluated using the χ^2 distribution and the Schwartz criterion of parsimony reported by Pierpaoli and Jones (29).

Restricted and Nonrestricted Diffusion

van Gelderen et al. (2) derived the following expression for the attenuation of an MR signal in a Stejskal–Tanner type experiment due to the diffusion of spins confined to the interior of an infinite cylinder:

$$\ln\left(\frac{A_\perp}{A_0}\right) = -2\gamma^2 g^2 \sum_{m=1}^{\infty} \frac{2D_i\alpha_m^2\delta - 2 + 2e^{-D_i\alpha_m^2\delta} + 2e^{-D_i\alpha_m^2\Delta} - e^{-D_i\alpha_m^2(\Delta-\delta)} - e^{-D_i\alpha_m^2(\Delta+\delta)}}{D_i^2\alpha_m^6(R^2\alpha_m^2 - 1)}$$

$$= -F_{g,\delta,\Delta}(D_i, R), \qquad [1]$$

where $A_\perp$ is the signal measured with diffusion weighting gradient perpendicular to the cylinder axis, A_0 the signal without diffusion weighting, γ the gyromagnetic ratio, D_i the intracellular diffusion coefficient, R the radius of the cylinder, δ the gradient pulse duration, Δ the gradient pulse separation, g the gradient pulse amplitude, and α_m the mth root of the equation:

$$J_1'(\alpha_m R) = 0 \qquad [2]$$

where J_1' is the derivative of the Bessel function of the first kind and order 1. They then used this equation to estimate the size of the compartment restricting the diffusion of phosphocreatine in the leg muscle of a rabbit. Meier et al. (20,21) used the same model to estimate the radius of the cylindrical intracellular compartments in rat brain tissue.

While the above model appears adequate to describe the restricted diffusion in the intracellular compartment, it does not include the diffusion in the extracellular com-

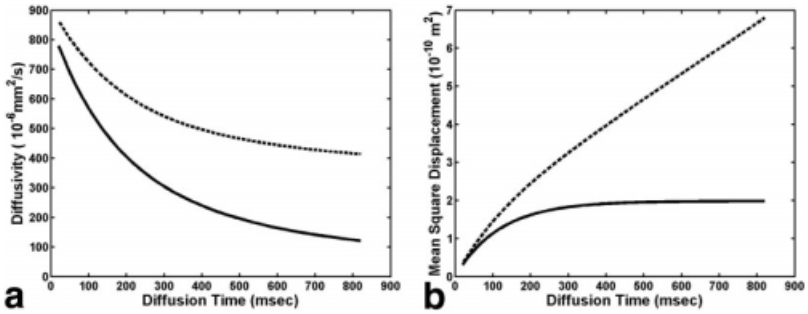

FIG. 1. Apparent diffusivity $D_\perp$ (**a**) and mean square displacement $\langle x^2 \rangle$ (**b**) versus diffusion time τ_d for the one-compartment (solid line) and two-compartment (dashed line) models. The models are described by Eq. [5] with $R = 20$ μm, $D_i = D_n = 1000 \times 10^{-6}$ mm^2/s, and $\rho = 1$ (one compartment) and $\rho = 0.6$ (two compartment). The mean square displacement, apparent diffusivity, and diffusion time are related by $\langle x^2 \rangle = D_\perp \tau_d$. In the one-compartment model, all the diffusing particles are confined inside the cylinders, so $\langle x^2 \rangle \rightarrow R^2/2$ and $D_\perp \approx R^2/2\tau_d$ as $\tau_d \rightarrow \infty$. In contrast, for the two-compartment model in the same limit, $D_\perp$ increases without bound and $D_\perp$ approaches a nonzero asymptote.

partment nor the exchange through the permeable membrane. To include the extracellular spins in our model, we propose that the MR signal is the sum of the signal from restricted spins described by Eq. [1] and nonrestricted spins described by the Stejskal–Tanner formula:

$$\begin{aligned} A_\perp/A_0 &= \rho e^{-F_{g,\delta,\Delta}(D_i,R)} + (1-\rho)e^{-\gamma^2 g^2 \delta^2 (\Delta - \delta/3) D_n} \\ &= \rho e^{(-F_{g,\delta,\Delta}(D_i,R)} + (1-\rho)e^{-bD_n} \end{aligned} \quad [3]$$

where ρ is the volume fraction of the intracellular compartment and D_n the nonrestricted diffusion in the extracellular space. Equation [3] is similar to the two-compartment model of Pfeuffer et al. (19), who used a lattice model instead of a cylindrical model for the restricted compartment.

Although it is difficult to measure $A_\perp$ directly for individual muscles or muscle groups with different orientations, it is straightforward to formally compute $D_\perp$, the apparent diffusion constant perpendicular to the cylinder axis, from the data by diagonalizing the diffusion tensor. $D_\perp$ and $A_\perp$ are formally related by

$$A_\perp = A_0 \exp(-b_\perp D_\perp). \quad [4]$$

Using Eqs. [3] and [4], $D_\perp$ can be expressed as

$$D_\perp = -\ln\{\rho \exp(-F_{g,\delta,\Delta}(D_i,R)) + (1-\rho)\exp(-bD_n)\}/b. \quad [5]$$

The combined diffusion model and the restricted diffusion model ($\rho = 1$) are compared in Fig. 1. Figures 1a and b show $D_\perp$ versus τ_d and the mean square displacement versus τ_d, respectively, for the combined diffusion model (dashed line) and the restricted diffusion model (solid line). $D_\perp$ decreases with increasing τ_d for both models. This agrees with the result of Gates and Cameron (30) that the apparent diffusion coefficient perpendicular to the fibers is inversely proportional to the square root of τ_d. As τ_d tends to infinity, the presence of the impermeable boundary limits the mean square displacement for the restricted model to $R^2/2$ (2), and $D_\perp$ approaches 0. In contrast, the particles in the external compartment in the combined model are still free to diffuse. Thus, for the combined model, the mean square displacement increases without bound, and $D_\perp$ approaches a nonzero value.

Interpretation of the data are straightforward for regions where the muscle fibers are parallel: the diffusion ellipsoid is a prolate spheroid; λ_2 and λ_3 (presumably equal) describe diffusion perpendicular to the fiber axis; and λ_1, which describes diffusion along the fiber axis, should not depend on τ_d. Interpretation of data from regions where fibers cross is not as straightforward. In both the heart and the tongue core region, the fiber bundles are laminar. One principal axis of the diffusion ellipsoid is normal to the plane of the fibers. If the fibers all have the same diameter (an assumption, not rigorously satisfied, implicit in Eq. [4]) and are either perpendicular to each other or are uniformly distributed in azimuth, the diffusion ellipsoid is an oblate spheroid, with $\lambda_1 = \lambda_2$ describing diffusion in the plane of the fibers and λ_3 describing diffusion perpendicular to the plane of the fibers. The mid part of the intrinsic tongue core is such a region, as indicated by histologic study of the tongue (31). In all other cases, the three eigenvalues will be distinct.

Our fitting procedure consisted of the following steps:

1. Computation of diffusion tensor for diffusion times for all pixels in images that contained tissue;
2. Manual selection of an ROI containing more than 100 pixels from anatomically uniform regions;
3. Random selection of 90% of the pixels from the ROI;
4. Averaging of each eigenvalue for the selected pixels for each diffusion time;
5. Fitting of each average eigenvalue to Eq. [4], using the Nelder–Mead simplex algorithm (32) to extract the parameters ρ, D_i, D_n, and R;
6. A total of 99 repetitions of steps 3–5 to obtain other estimates of the parameters;
7. Calculation of means and standard deviations of the values of parameters;
8. Repetition of steps 2–7 for a different tissue type.

RESULTS

The complex myoarchitecture of the ex vivo calf heart is shown in Fig. 2a, which consists of DEC maps of λ_1 and its

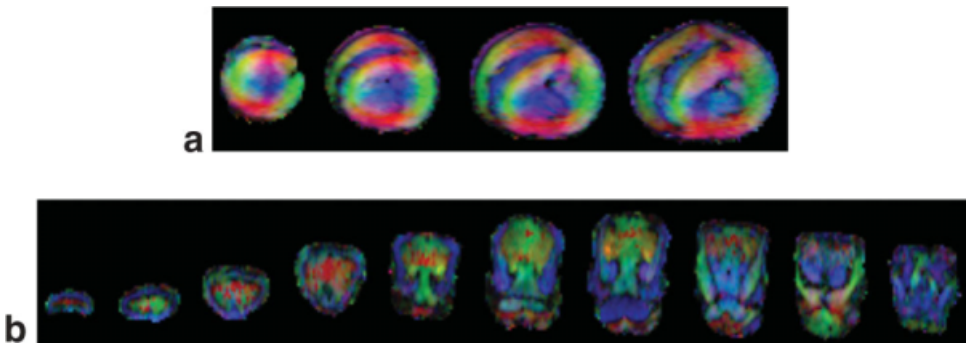

FIG. 2. Myoarchitecture of heart (**a**) and tongue (**b**), depicted by DEC maps. These maps were computed from diffusion tensor images acquired with $\tau_d = 200$ ms. The color indicates the direction of $\mathbf{v}_1$, the eigenvector corresponding to the largest eigenvalue; red is left–right, green is up–down, and blue is through-plane. The brightness is proportional to the lattice index. (a) Four short axis images of the heart; the image on the left is closest to the apex. (b) Ten coronal images of the tongue; the leftmost image is closest to the anterior tip. The DEC maps delineate different muscles and their fiber orientations.

eigenvector $\mathbf{v}_1$. The slices shown represent the short axis of the heart. The heart muscles lie on nested shells surrounding each ventricle. The angle between the muscle fiber direction and the slices shown increases toward the inside of the ventricle. This is clearly seen in the left ventricle, where the fibers appear in red and green (in plane) near the outer surface and in blue (through plane) near the inner surface.

The complexity of lingual myoarchitecture is shown in Fig. 2b. The muscle depicted in blue at the bottom of slices 6 and 8 (counting from left to right) is the geniohyoid. On top of the geniohyoid in the same slices are the genioglossus in the middle and the hyoglossus on the sides. The intrinsic tongue core occupies the upper one-third to one-half of the tongue above the genioglossus. The tongue core, appearing in random patches of red and green, is uniquely identified with negative skewness because of the interdigitation of vertical and transverse muscles in a laminar pattern. It should be emphasized that an area of a particular color does not necessarily represent either the vertical or the transverse muscle individually; along which muscle $\mathbf{v}_1$ points depends on the volume fraction of two interwoven muscles. In addition, if the underlying tensor is nearly isotropic, the azimuthal angle of $\mathbf{v}_1$ will be random.

Diffusion-Time-Dependent Diffusivity

The ROIs in three different anatomic regions were chosen for analysis. The locations of these representative ROIs were: in the left ventricle (Fig. 3a); in the genioglossus (Fig. 3b); and in the tongue core (Fig. 3c). Note that the anatomic characteristics of the genioglossus and the tongue core are very different. The genioglossus consists of parallel fibers, while the tongue core consists of fibers that cross. The DEC and SK images were used to select ROIs that reflect different muscle fiber characteristics. Figures 3d–f show λ_1, λ_2, and λ_3 as functions of τ_d for the three target tissues. Each point plotted is the average of an eigenvalue over all the pixels in all the ROIs for a particular target tissue. The error bars are the SD of the eigenvalues included in the average. Figures 3d and e, respectively, depict the heart and the genioglossus, regions containing parallel fibers. In these regions λ_2 and λ_3, which correspond to diffusion perpendicular to the fiber axis, are functions of τ_d, while λ_1, which represents diffusion parallel to the fiber axis, is almost independent of τ_d. Figure 3f depicts the tongue core, a region consisting of a laminar structure of crossing fibers. In this region, all three eigenvalues decreased as τ_d increased, but λ_1 and λ_2, which represent diffusion in the plane of the fibers, decreased less than λ_3, which represents diffusion perpendicular to the plane of the fibers. As expected, the τ_d dependency of λ_3 was the same for all target tissues, while the τ_d dependency of λ_1 and λ_2 in the tongue core resembled the average of λ_1 and λ_2 in the genioglossus and the left ventricle.

Table 1 contains the eigenvalues and trace of the diffusion tensors, plus three anisotropy measures (FA, SK, and LI) at diffusion times 33, 115, and 412 ms for all three target tissues. The percentage change was computed in the eigenvalues between $\tau_d = 33$ ms and the longer times for each target tissue. The significance of the change was tested using Student's *t* test.

The changes of λ_2 and λ_3 between $\tau_d = 33$ and 115 ms and between $\tau_d = 33$ and 412 ms were significant for all target tissues, as were the changes in λ_1 in the tongue core ($P < 0.001$). The changes in λ_1 for the heart and the genioglossus were not significant ($P > 0.01$), except for the small (3.6%) change in the value of λ_1 of heart muscle between $\tau_d = 33$ and 115 ms ($P = 0.0002$). Note that this change is much smaller than the 20% change in the other eigenvalues. It is interesting to note that the percentage changes in λ_2 and λ_3 in the heart were as large as those in the genioglossus, 17–27% between $\tau_d = 33$ and 115 ms and 28–36% between $\tau_d = 33$ and 412 ms, while the increases of FA and SK in the heart muscle were always smaller than those in the genioglossus by 10–100%. This difference can be attributed to the magnitude of λ_2 and λ_3 compared with that of λ_1 at diffusion time 33 ms. The λ_2 of the heart muscle is about half of λ_1, while the λ_2 of the genioglossus is about 74% of λ_1. Thus, the changes in the λ_2 and λ_3 of the heart muscle contribute less to the change of FA and SK than those of the genioglossus. The degree of anisotropy increase may also be responsible for the increase of LI, the intervoxel anisotropy, as the uncertainty of fiber direction due to noise may decrease by the increase of anisotropy (33).

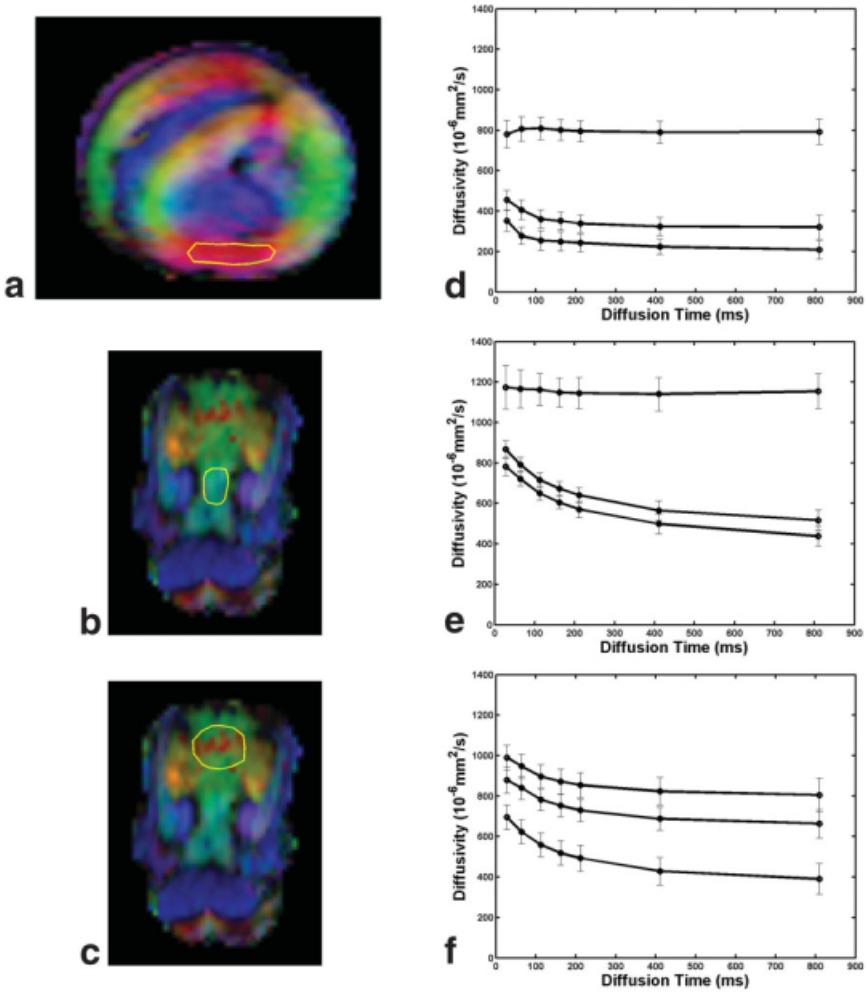

FIG. 3. Locations of typical ROIs and plots of eigenvalues of the apparent diffusion tensor versus τ_d in heart (**a** and **d**) genioglossus, (**b** and **e**) and tongue core (**c** and **f**). Several ROIs were selected in the left ventricle. The ROI of the genioglossus does not include the region where the genioglossus emerges from the tongue core. The tongue core ROI is confined to the middle of the muscle group, as shown, where the amounts of vertical and transverse fibers are about equal. The lines connecting the points in the plots are trend lines, not fit results. The error bars denote the standard deviations of the distribution of values in the ROI. Note that λ_2 and λ_3 decrease in all three target tissues, while λ_1 decreases only in the tongue core.

Model-Based Analysis

The results of fitting the data for λ_2 of the genioglossus to Eq. [4] are shown in Fig. 4a. The fit was excellent. Figure 4b shows the corresponding mean square displacement plotted versus τ_d. The shape of the curve was the same as that in Fig. 1b, demonstrating that both the restricted and the unrestricted components were present. Analogous fits were performed for all eigenvalues that showed restriction; the resulting fit parameters are shown in Table 2. The errors were computed using the "bootstrap method" described under Methods.

The estimated volume fraction of the restricted compartment averaged 0.65 in the heart and 0.43 in the genioglossus; in the tongue core, it was 0.21 for λ_1, 0.25 for λ_2, and 0.45 for λ_3. The results in the tongue core are easily explained. Since λ_3 describes diffusion perpendicular to all the fibers, the associated volume fraction is similar to the volume fraction in the genioglossus. Although λ_1 and λ_2

Table 1
Eigenvalues and Trace of the Diffusion Tensor and Anisotropy Measures for Heart, Genioglossus, and Tongue Core for τ_d = 33, 115, and 412 ms

	Diffusion time (ms)	Diffusivity (10^{-6} mm^2/s)				Anisotropy measures ($\times 10^{-3}$)		
		λ_1	λ_2	λ_3	Trace	FA	LI	SK
Heart	33	781 ± 68	455 ± 49	353 ± 51	1589 ± 121	400 ± 73	254 ± 52	5.7 ± 3.0
	115	809 ± 56	361 ± 45	256 ± 48	1426 ± 95	552 ± 70	395 ± 62	14.3 ± 5.2
	412	790 ± 55	324 ± 45	224 ± 39	1339 ± 80	592 ± 63	434 ± 60	17.2 ± 5.9
Genioglossus	33	1174 ± 108	867 ± 43	782 ± 46	2824 ± 151	216 ± 49	116 ± 25	1.1 ± 0.9
	115	1163 ± 79	715 ± 36	650 ± 35	2528 ± 89	319 ± 51	198 ± 33	3.7 ± 1.7
	412	1141 ± 83	565 ± 48	499 ± 49	2204 ± 71	446 ± 75	307 ± 55	9.4 ± 4.0
Tongue core	33	990 ± 61	879 ± 64	695 ± 60	2565 ± 127	176 ± 50	91 ± 29	−0.3 ± 0.6
	115	897 ± 58	783 ± 54	559 ± 59	2239 ± 119	230 ± 52	130 ± 33	−0.8 ± 0.9
	412	823 ± 69	688 ± 57	430 ± 69	1941 ± 127	304 ± 70	184 ± 49	−1.8 ± 2.1

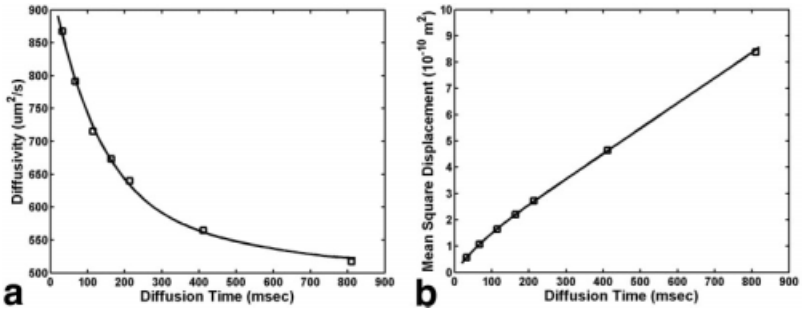

FIG. 4. Example of model fitting to measurement data. λ_3 (**a**) and (**b**) versus τ_d for the genioglossus and the results of fitting the data to Eq. [5]. The model parameters of the best fit were $\rho = 0.42$, $R = 16.37$ μm, $D_i = 1158 \times 10^{-6}$ mm²/s, and $D_n = 947 \times 10^{-6}$ mm²/s.

describe diffusion in the plane of the fibers, in that plane only about half the fibers are oriented with their axis perpendicular to the eigenvector $\mathbf{v}_1$ (or $\mathbf{v}_2$). The axis of the other half of the fibers lies along $\mathbf{v}_1$ (or $\mathbf{v}_2$), so the diffusion in those fibers is not restricted. The inferred volume fraction of the restricted compartment is therefore half the true volume fraction.

The estimated radius of the restricting cylinders was about 6.25–6.55 μm in the heart and 13.7–17.8 μm in the genioglossus and tongue core. In the heart, the estimated intracellular diffusivity, D_i, was much less than the diffusivity in the nonrestricted compartment, $D_{n,,}$ whereas in the genioglossus and tongue core D_i was larger than D_n. Comparison of the different target tissues showed D_i in the heart to be only half as large as that in the tongue.

Experiments to Control for Potential Confounds

Effects of Echo Time (TE)

Figure 5 shows the results of diffusion tensors computed from images acquired with constant width and constant amplitude of the diffusion sensitizing gradients. The results from the two acquisition modalities were in excellent agreement, indicating that the variable TE (constant amplitude) used for most of our experiments did not affect the diffusion findings. In particular, both modalities showed the same degree of diffusivity changes as a function of diffusion time.

Temperature Effects

The eigenvalues of the diffusion tensors were computed from each of the eight replicates collected over the course of the entire experiment in an ROI in the heart with 528 voxels. Although the uncertainties in the parameter values are large due to computation from a single replicate, no systematic differences between data acquired early and late in the scanning session were large enough to alter our results. The λ_2 and λ_3 with diffusion time longer than 200 ms did increase by about 10% (0.3×10^{-4} mm²/s) at maximum during the eight repetitions. However, this effect was small compared to the overall decrease (about 1.3×10^{-4} mm²/s) of λ_2 and λ_3 as a function of diffusion time.

Assumption of Monoexponential Decay

Results of the multiple *b*-value experiments showed no significant deviation from a monoexponential decay of the signal as a function of *b*, indicating that a single tensor model fitted the data quite well. However, the parsimony criterion of Schwartz indicated that the best model to fit the data in more than 85% of voxels in both tongue and heart would be the combination of one anisotropic tensor and one isotropic tensor with fixed diffusivity close to free water diffusion. Similar results have been observed recently in DTI of the human living brain (29). The volume fraction of this isotropic compartment was less than 10%.

DISCUSSION

The present study represents the first to substantiate the selective dependence of water diffusion tensor on diffusion time in ex vivo calf tongue and heart muscle tissues. Our findings showed that the eigenvalues of the diffusion

Table 2
Compartment Radius *R,* Intracellular Diffusivity D_i, Extracellular Diffusivity D_n, and Volume Fraction ρ Derived from Fitting the Eigenvalues of the Diffusion Tensor as a Function of Diffusion Time with the Two-Compartment Model (Eq.[5]) for *ex Vivo* Heart, Genioglossus, and Tongue Core

	ρ	*R* (μm)	D_i (10^{-6} mm²/s)	D_n (10^{-6} mm²/s)
Heart				
λ_2	0.63 ± 0.05	6.55 ± 0.20	477 ± 78	1110 ± 223
λ_3	0.67 ± 0.04	6.25 ± 0.18	497 ± 80	770 ± 97
Genioglossus				
λ_2	0.42 ± 0.01	16.38 ± 0.15	1162 ± 32	945 ± 18
λ_3	0.43 ± 0.02	17.76 ± 0.34	1173 ± 71	772 ± 30
Tongue-core				
λ_1	0.21 ± 0.01	13.72 ± 0.20	1160 ± 46	1092 ± 13
λ_2	0.25 ± 0.04	15.73 ± 1.16	1302 ± 271	931 ± 85
λ_3	0.45 ± 0.01	14.65 ± 0.07	1030 ± 13	725 ± 7

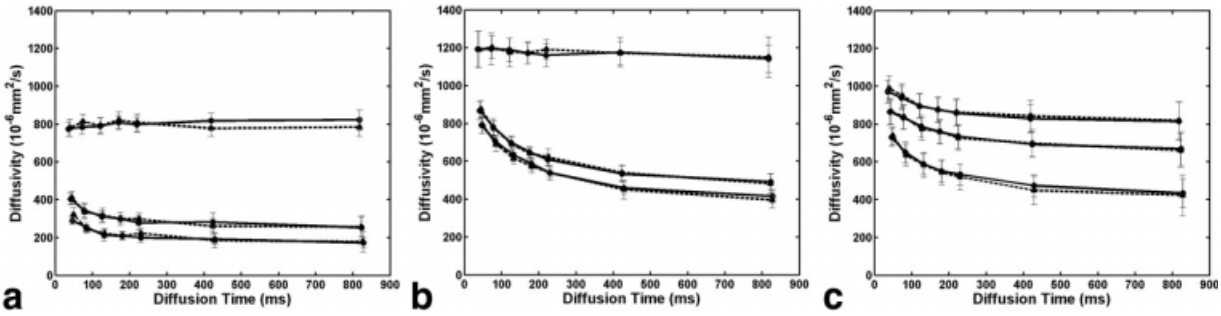

FIG. 5. Eigenvalues of the apparent diffusion tensor from data collected with diffusion pulse of constant duration (triangles, dashed lines) and constant amplitude (circles, solid lines) versus τ_d. The error bars denote the standard deviations of the distribution of values in the ROI. Note the excellent agreement between the corresponding measurements.

tensor, and therefore quantities derived from them, such as the trace and anisotropy indices, were all a function of τ_d. In regions where the muscle fibers are parallel (skewness is positive and diffusion ellipsoid is prolate), λ_1, which describes diffusion parallel to the fiber axis, had no diffusion time dependence, whereas λ_2 and λ_3, which describe diffusion perpendicular to the fiber axis, decreased with increasing diffusion time. Diffusion anisotropy computed from images acquired with long diffusion times is therefore much larger than that computed from images acquired with short diffusion times. Using bootstrap methods, Jones (33) demonstrated an inverse relationship between the anisotropy of the tissue and the uncertainty in the determination of the direction of the eigenvector corresponding to the largest eigenvalue. Diffusion measurements of the muscle fiber orientation should therefore use long diffusion times to increase tissue anisotropy and thereby reduce the uncertainty in the estimated direction of fibers. On the other hand, longer diffusion time will result in decreased signal-to-noise ratio (SNR) in the acquired images in any pulse sequence. Thus, a reasonable trade-off between SNR and anisotropy should be made to achieve the optimal result in practical applications.

There are only a limited number of DTI studies reported for in vivo heart and tongue. The myocardial diffusion eigenvalues measured with the shortest diffusion time (33 ms) in our study are in a range similar to that of the values measured in a human study by Dou et al. (11) where they used diffusion times between 13 and 26 ms. About 10% higher diffusivity along the first eigenvector direction in human data could be due to anatomic difference between human and calf cardiac myofibers as well as increased temperature and noise under in vivo situations. The tongue DTI data measured with long diffusion times (>400 ms) in our study is in good agreement with the ex vivo calf tongue DTI data reported by Wedeen et al. (14) measured with 500-ms diffusion time. Average diffusivities measured in previous DTI studies of in vivo skeletal muscles (6,7) are about 1.1×10^{-5} cm^2/s for rat lateral gastrocnemius (τ_d = 12.5 ms) and 1.8×10^{-5} cm^2/s for human calf muscle (τ_d = 29.3 ms). The mean diffusivity of the ex vivo lingual muscle with similar diffusion time (33 ms) in our study is about 0.94 ($\pm$0.05) $\times 10^{-5}$ cm^2/s. Considering the difference in temperature and myofiber size, they appear to be in a reasonably similar range.

Two aspects of the present study were unique: multiple checks for potential confounds and the use of a four-parameter analytical model. In relatively complicated experiments such as ours, it is important to check for potential confounds that may affect results. Our multiple, carefully designed checks have confirmed that the detected diffusion time dependence was not a spurious finding caused by systematic errors in the STEAM sequence, temperature changes during the long scan, unaccounted contributions of the imaging gradients to diffusion sensitization, effects of the variable echo time, or failure of the tensor model to fit the data. Our use of a four-parameter (volume fraction ρ, intracellular diffusivity D_i, extracellular diffusivity D_n, and fiber radius R) model for analysis, which consists of a linear combination of a cylindrically restricted diffusion compartment and a nonrestricted diffusion compartment, proved to be effective. The model fitted our data well, and we were able to obtain reliable estimates of the model parameters.

Our estimates of myofiber diameters in the calf heart and tongue were 6.25–6.55 and 13.7–17.8 μm, respectively. Fiber diameters from past histologic studies were 6–12 μm for human heart muscle (35), 20–40 μm for lingual muscles of monkey (36), 30–50 μm for human tongue muscles (37), and 30–60 μm for beef chuck (38). Jointly, these findings indicate that cardiac muscles fibers are considerably smaller than lingual muscle fibers and that this difference in size persists across species (calf versus human) and study modalities (DTI versus histology). It is noted that our analysis is based on the assumption of homogeneous arrangement of restricting compartments within imaging voxels, as it is not possible to have high enough spatial resolution to image individual restricting compartments using currently available clinical MR scanners. Particularly for the tongue core region with complex fiber crossings, it may require higher spatial resolution and a larger number of diffusion gradient directions to improve the accuracy of the measurement. This remains for future study.

We also found the extracellular diffusivity of both heart and tongue muscles to be almost the same, implying that the extracellular medium is similar in the muscles of these different organs. Intracellular diffusivity, on the other hand, differed greatly in cardiac and lingual myofibers. The intracellular diffusion of heart muscle was only about

half of that of tongue muscle due perhaps to the difference in striation patterns and other cellular structural characteristics. Moreover, we found the intracellular volume fraction of tongue and heart myofiber to be quite different: $\rho \sim 43\%$ in the tongue (genioglossus and tongue core) compared to ~65% in the heart. The volume fraction of the intracellular space of tongue muscle is in good agreement with published histologic finding of an average 44.41% of muscle concentration in the corresponding sites (34). Further studies are required to elucidate how this finding is related to the physiologic functions of the muscles of the two organs.

Recently, a similar model was introduced by Assaf et al. (39) that describes restricted and hindered water diffusion in brain tissue with a combination of an asymptotic form of cylindrically restricted diffusion and an effective diffusion tensor. They used the model to estimate the orientations of crossing fibers. Their restricted diffusion model is based on the assumption of constant gradient waveform (diffusion time ~ diffusion gradient duration) during their measurement. Because our experiment used long diffusion time and relatively short gradient pulses, this assumption does not hold for the entire range of our experimental conditions. Our model is apparently better suited for the analysis of the diffusion time dependence of water diffusion. It is also possible to expand our model to have multiple restricted and nonrestricted compartments if enough measurements are available.

It should be pointed out that our approach had one inconsistency. For every value of τ_d, the elements $D_{ij}(\tau_d)$ of a single diffusion tensor were computed by fitting the image data to an expression of the form

$$A(b_{ij}) = A_0 \exp(-b_{ij}D_{ij}(\tau_d)), \quad [6]$$

where $A(b_{ij})$ is the observed signal, A_0 is the signal in the absence of diffusion attenuation, the elements of the b-matrix are determined by the timing of the pulse sequence, and the apparent diffusion tensor **D** is a function of the diffusion time τ_d. Parameters derived from the elements of **D** were then fitted to Eq. [4], which contains two diffusion parameters, D_i and D_n. The question remains: how can the signal have such complicated dependence on τ_d and such a simple dependence on b?

Several investigators have performed experiments to determine the conditions for which Eq. [6] accurately describes the b-dependence of the diffusion attenuation. A simple modification is to add an extra term to the right side of Eq. [6]:

$$A(b_{ij}) = A_0(\alpha\exp(-b_{ij}D_{ij}^{[1]}(\tau_d)) + (1-\alpha)\exp(-b_{ij}D_{ij}^{[2]}(\tau_d))). \quad [7]$$

Inglis et al. (40) found the biexponential model to be more accurate for b-values up to 9000 s/mm^2. Meier et al. (21) found that a third term improves the fit for b-values up to 580000 s/mm^2. However, Niendorf et al. (18) had similar findings to ours in their study of a healthy rat brain at a diffusion time of less than 6 ms; for b values up to 1500 s/mm^2, they held b constant and observed the signal attenuation decrease with increasing diffusion time, yet for each value of τ_d, the signal attenuation as a function of b was well described by a single exponential. A later experiment has demonstrated that the signal decay is biexponential if much larger b-values are used (9000 s/mm^2) and the signal decay at b-values less than 1500 s/mm^2 appears monoexponential because, at low b-values, decay is dominated by the fast diffusion component (40). Had we performed the experiments with larger b-values, we might have observed biexponential decay; however, the relatively low SNR achievable on a clinical scanner precluded this option.

The imaging and analysis techniques employed in the present study have the potential for noninvasive measurement of changes in the biomechanical properties of muscles. Previous studies support the feasibility to observe diffusion time-dependent water diffusion under in vivo conditions, similar to what we observed in ex vivo model. Latour et al. (41) have shown the diffusion time dependency of water diffusion in isolated red blood cells with different packing densities and membrane permeabilities. Meier et al. (21) reported that the intracellular exchange times of fresh postmortem rat brain were about 8% lower than those of the corresponding in vivo brains based on their measurements with diffusion times longer than 780 ms. Thus, we expect that our observations with fresh postmortem tissues may closely resemble what one could observe with in vivo muscle tissues. Future clinical applications may include the monitoring of disease progression and the assessment of therapeutic effects of drugs and exercise on muscle tissue characteristics. However, before such applications can be implemented in vivo with human subjects, significant reduction of scanning time and efficient control of potential sources of artifacts such as motion must be achieved. Recent development of parallel imaging methodology in conjunction with partial k-space sampling may present solutions for overcoming current technical barriers.

CONCLUSIONS

The present study shows that the apparent diffusion tensor of water measured in ex vivo muscle tissues depends on the diffusion time used in the experiment. To our knowledge, it is the first demonstrating diffusion time dependence of measured water diffusion tensor in muscular tissue. In contrast to brain tissue where prohibitively short diffusion times must be used (less than 6 ms), in muscles this phenomenon can be observed over a range of diffusion times achievable on a clinical MR scanner. Muscle fiber diameter, volume fraction, and intra/extracellular diffusivities can be adequately estimated by fitting the eigenvalues of the apparent diffusion tensor to a proposed two-compartment model. With improvement in scanning technology, DTI holds promise for noninvasive, quantitative detection of in vivo changes in muscle myoarchitecture due to disease, treatment, and exercise.

ACKNOWLEDGMENTS

The authors thank Dr. Peter Basser for providing insightful comments on the paper. The Physical Disabilities Branch is a collaboration between the National Institute of Child

Health and Human Development and the Clinical Research Center, NIH. The opinions presented in this report reflect the views of the authors and not those of the National Institutes of Health nor the US Public Health Service.

REFERENCES

1. Cleveland GG, Chang DC, Hazlewood CF, Rorschach HE. Nuclear magnetic resonance measurement of skeletal muscle. Biophys J 1976;16: 1043–1053.
2. van Gelderen P, DesPres D, van Zijl PCM, Moonen CTW. Evaluation of restricted diffusion in cylinders. Phosphocreatine in rabbit leg muscle. J Magn Reson B 1994;103:255–260.
3. Kinsey ST, Locke BR, Penke B, Moerland TS. Diffusional anisotropy is induced by subcellular varriers in skeletal muscle. NMR Biomed 1999; 12:1–7.
4. Basser PJ, Mattiello J, Le Bihan D. MR diffusion tensor spectroscopy and imaging. Biophys J 1994;66:259–267.
5. van Donkelaar CC, Kretzers LJ, Bovendeerd PH, Lataster LM, Nicolay K, Janssen JD, Drost MR. Diffusion tensor imaging in biomechanical studies of skeletal muscle function. J Anat 1999;194:79–88.
6. Sinha U, Yao L. In vivo diffusion tensor imaging of human calf muscle. J Magn Reson Imaging 2002;15:87–95.
7. Damon BM, Ding Z, Anderson AW, Freyer AS, Gore JC. Validation of diffusion tensor MRI-based muscle fiber tracking. 2002;48:97–104.
8. Holmes AA, Scollan DF, Winslow RL. Direct histological validation of diffusion tensor MRI in formaldehyde-fixed myocardium. Magn Reson Med 2000;44:157–161.
9. Scollan DF, Holmes A, Zhang J, Winslow RL. Reconstruction of cardiac ventricular geometry and fiber orientation using magnetic resonance imaging. Ann Biomed Eng 2000;28:934–944.
10. Winslow RL, Scollan DF, Greenstein JL, Yung CK, Baumgartner Jr W, Bhanot G, Gresh DL, Rogowitz BE. Mapping, modeling, and visual exploration of structure-function relationships in the heart. IBM Syst J 2001;40:342–359.
11. Dou J, Reese TG, Tseng WYI, Wedeen VJ, Cardiac diffusion MRI without motion effects. Magn Reson Med 2002;48:105–114.
12. Chen J, Wong SK, Liu W, McLean M, Allen JS, Tan J, Wickline SA, Yu X. Remodeling of cardiac fiber structure after infarction in rats quantified with diffusion tensor MRI. Am J Physiol 2003;285 (Heart Circ Physiol):H946–H954.
13. Gilbert RJ, Reese TG, Daftary SJ, Smith RN, Weisskoff RM, Wedeen VJ. Determination of lingual myoarchitecture in whole tissue by NMR imaging of anisotropic water diffusion. Am J Physiol 1998; 275 (Gastrointest Liver Physiol 38): G363–G369.
14. Wedeen VJ, Reese TG, Napadow VJ, Gilbert RJ. Demonstration of primary and secondary muscle fiber architecture of the bovine tongue by diffusion tensor magnetic resonance imaging. Biophys J 2001;80:1024–1028.
15. Napadow VJ, Chec Q, Mai V, So PTC, Gilbert RJ. Quantitative analysis of three-dimensional-resolved fiber architecture in heterogeneous skeletal muscle tissue using NMR and optical imaging methods. Biophys J 2001;80:2968–2975.
16. Woessner DE. NMR spin-echo self-diffusion measurements on fluids undergoing restricted diffusion. J Phys Chem 1963;67:1365–1367.
17. Crick F. Diffusion in embryogenesis. Nature 1970;5231:420–422.
18. Niendorf T, Norris DG, Leibfritz D. Detection of apparent restricted diffusion in healthy rat brain at short diffusion times. Magn Reson Med 1994;32:672–677.
19. Pfeuffer J, Flogel U, Dreher W, Leibfritz D. Restricted diffusion and exchange of intracellular water: theoretical modelling and diffusion time dependence of ^{1}H NMR measurements on perfused glial cells. NMR Biomed 1998;11:19–31.
20. Meier C, Dreher W, Leibfritz D. Diffusion in compartmental systems. I. A comparison of an analytical model with simulations. Magn Reson Med 2003;50:500–509.
21. Meier C, Dreher W, Leibfritz D. Diffusion in compartmental systems. II. Diffusion-weighted measurements of rat brain tissue in vivo and postmortem at very large b-values Magn Reson Med 2003;50:510–514.
22. Jones DK, Basser PJ, Squashing peanuts and smashing pumpkins: how noise distorts diffusion-weighted MR data. In: Proceedings of the 12th Annual Meeting of ISMRM, Kyoto, Japan, 2004. p 86.
23. Basser PJ, Pierpaoli C. Microstructural features measured using diffusion tensor imaging. J Magn Reson B 1996;111:209–219.
24. Conturo TE, McKinstry RC, Akbudak E, Robinson BH, Encoding of anisotropic diffusion with tetrahedral gradients: A general mathematical diffusion formalism and experimental results. Magn Reson Med 1996;35:399–412.
25. Pierpaoli C, Basser PJ. Toward a quantitative assessment of diffusion anisotropy. Magn Reson Med 1996;36:893–906.
26. Pajevic S, Pierpaoli C. Color schemes to represent the orientation of anisotropic tissues from diffusion tensor data: application to white matter fiber tract mapping in the human brain. Magn Reson Med 1999;42:526–540.
27. Bland KM, Altman DG. Measuring agreement in method comparison studies. Stat Methods Med Res 1999;8:135–160.
28. Jones DK, Horsfield MA, Simmons A. Optimal strategies for measuring diffusion in anisotropic systems by magnetic resonance imaging. Magn Reson Med 1999;42:515–525.
29. Pierpaoli C, Jones DK. Removing CSF contamination in brain DT-MRIs by using a two-compartment tensor model. In: Proceedings of the 12th Annual Meeting of ISMRM, Kyoto, Japan, 2004. p 1215.
30. Gates L, Cameron I. Time dependent diffusion coefficients of water within hollow fibers. In: Proceedings of the 3rd Annual Meeting of ISMRM, Nice, France, 1995. p 355.
31. Takemoto H. Morphological analyses of the human tongue musculature for three-dimensional modeling. J Speech Language Hearing Res 2001; 44:95–107.
32. Lagarias JC, Reeds JA, Wright MH, Wright PE. Convergence properties of the Nelder-Mead simplex method in low dimensions. SIAM J Optimiz 1998;9:112–147.
33. Jones DK. Determining and visualizing uncertainty in estimates of fiber orientation from diffusion tensor MRI. Magn Reson Med 2003;49:7–12.
34. Miller JL, Watkin KL, Chen MF. Muscle, adipose, and connective tissue variations in intrinsic musculature of the adult human tongue. J Speech Language Hearing Res 2002;:51–65.
35. Snir M, Kehat I, Gepstein A, Coleman R, Itskovitz-Eldor J, Livne E, Gepsteain L. Assessment of the ultrastructural and proliferative properties of human embryonic stem cell-derived cardiomyocytes. Am J Physiol Heart Circ Physiol 2003;285:H2355–H2363.
36. DePaul R, Abbs JH. Quantitative morphology and histochemistry of intrinsic lingual muscle fibers in Macaca fascicularis. Acta Anat 1996; 155:29–40.
37. Stal P, Marklund S. Thornell LE, DePaul R. Eriksson PO. Fiber composition of human intrinsic tongue muscles Cells Tissues Organs 2004; 173:147–161.
38. Kirchofer KS, Calkins CR, Gwartney BL. Fiber-type composition of muscles of the beef chuck and round. J Anim Sci 2002;80:2872–2878.
39. Assaf Y, Freidlin RZ, Rohde GK, Basser PJ. A new modeling and experimental framework to characterize hindered and restricted water diffusion in brain white matter. In: Proceedings of the 12th Annual Meeting of ISMRM, Kyoto, Japan, 2004. p 251.
40. Inglis BA, Bossart EL, Buckley DL, Wirth III ED, Mareci TH. Visualization of neuronal tissue water compartments using biexponential diffusion tensor MRI. Magn Reson Med 2001;45:580–587.
41. Latour LL, Svoboda K, Mitra PP, Sotak CH. Time-dependent diffusion of water in a biological model system. Proc Natl Acad Sci USA 1994; 91:1229–1233.